



Targeting uPA-uPAR interaction to improve intestinal epithelial barrier integrity in inflammatory bowel disease

Yang Cheng,^a Tyler R. Hall,^a Xiao Xu,^b Ivy Yung,^a Donald Souza,^a Jie Zheng,^a Felix Schiele,^c Matthias Hoffmann,^d M. Lamine Mbow,^a James P. Garnett,^e and Jun Li^{a*}

^aImmunology and Respiratory Diseases Research, Boehringer Ingelheim Pharmaceuticals, Ridgefield, CT, USA

^bComputational Biology Group, Discovery Research, Boehringer Ingelheim Pharmaceuticals, Ridgefield, CT, USA

^cBiotherapeutics Discovery, Boehringer Ingelheim Pharma GmbH & Co. KG, Biberach an der Riß, Germany

^dMedicinal Chemistry, Boehringer Ingelheim Pharma GmbH & Co. KG, Biberach an der Riß, Germany

^eImmunology and Respiratory Diseases Research, Boehringer Ingelheim Pharma GmbH & Co. KG, Biberach an der Riß, Germany

Summary

Background Loss of intestinal epithelial barrier integrity is a critical component of Inflammatory Bowel Disease (IBD) pathogenesis. Co-expression regulation of ligand-receptor pairs in IBD mucosa has not been systematically studied. Targeting ligand-receptor pairs which are induced in IBD mucosa and function in intestinal epithelial barrier integrity may provide novel therapeutics for IBD.

Methods We performed transcriptomic meta-analysis on public IBD datasets combined with cell surface protein-protein-interaction (PPI) databases. We explored primary human/mouse intestinal organoids and Caco-2 cells for expression and function studies of uPA-uPAR (prime hits from the meta-analysis). Epithelial barrier integrity was measured by Trans-Epithelial Electrical Resistance (TEER), FITC-Dextran permeability and tight junction assessment. Genetic (CRISPR, siRNA and KO mice) and pharmacological (small molecules, neutralizing antibody and peptide inhibitors) approaches were applied. Mice deficient of uPAR were studied using the Dextran Sulfate Sodium (DSS)-induced colitis model.

Findings The IBD ligand-receptor meta-analysis led to the discovery of a coordinated upregulation of uPA and uPAR in IBD mucosa. Both genes were significantly upregulated during epithelial barrier breakdown in primary intestinal organoids and decreased during barrier formation. Genetic inhibition of uPAR or uPA, or pharmacologically blocking uPA-uPAR interaction protects against cytokine-induced barrier breakdown. Deficiency of uPAR in epithelial cells leads to enhanced EGF/EGFR signalling, a known regulator of epithelial homeostasis and repair. Mice deficient of uPAR display improved intestinal barrier function *in vitro* and during DSS-induced colitis *in vivo*.

Interpretation Our findings suggest that blocking uPA-uPAR interaction via pharmacological agents protects the epithelial barrier from inflammation-induced damage, indicating a potential therapeutic target for IBD.

Funding The study was funded by Boehringer Ingelheim.

Copyright © 2021 The Authors. Published by Elsevier B.V. This is an open access article under the CC BY-NC-ND license (<http://creativecommons.org/licenses/by-nc-nd/4.0/>)

Keywords: IBD; Intestinal epithelial barrier; Organoid; uPAR; uPA

Introduction

The intestinal epithelial barrier provides a critical line of defence and crosstalk with the exogenous luminal environment. Dysfunction of the barrier is usually

associated with, and in many cases, a driving force of intestinal disease including Inflammatory Bowel Disease (IBD).^{1–3} Indeed, mucosal healing has drawn tremendous research attention and emerged as a critical endpoint in IBD clinical management.^{4–6} Identification of novel genes and pathways underlying mucosal healing would provide insights for IBD pathogenesis and therapeutic development.

*Corresponding author.

E-mail address: Jun.Li@Boehringer-Ingelheim.com (J. Li).
Current address:

Research in context

Evidence before this study

Studies have shown that a leaky, impaired epithelial barrier is a critical contributor to disease progression in Inflammatory Bowel Disease (IBD). Novel IBD drugs targeting epithelial barrier integrity are in great need to promote mucosal healing. Urokinase (uPA) is known to interact with its receptor uPAR and can mediate cell migration and activation. But the role of uPA-uPAR interaction in intestinal epithelial function related to IBD is unknown.

Added value of this study

This study applied a novel Protein-Protein-Interaction (PPI)-guided IBD transcriptomic meta-analysis and identified uPA-uPAR as a coordinately upregulated ligand-receptor pair in IBD biopsies. The coordinated upregulation was also observed in primary human intestinal organoids during epithelial barrier breakdown induced by pathogenic cytokines. We further provided functional validation showing that inhibition of uPAR or uPA genetically, or pharmacologically via PPI inhibitors protects against barrier damage in intestinal epithelial cells and organoids. Mice deficient of uPAR also displayed reduced epithelial damage in DSS-induced colitis. Overall, our study demonstrates the role of uPA-uPAR in regulating the intestinal barrier in IBD and highlights the therapeutic potential of uPA-uPAR for IBD mucosal healing.

Implications of all the available evidence

Our study highlights an important role of uPA-uPAR interaction and signalling in the intestinal epithelium and its therapeutic potential for IBD.

IBD-associated epithelial damage can be triggered by dysregulated communication between intestinal cells and their environment, which often requires signal transduction between cell surface receptors and their ligands. For instance, pro-inflammatory cytokines, such as TNF, IFN- γ , IL-6, IL-23, IL-22, IL-17, IL-18 and oncostatin M (OSM), play critical roles in IBD pathogenesis through receptor-mediated signalling and directly or indirectly regulate epithelial barrier integrity. Cytokine receptors on epithelial cells, such as IFN- γ R, IL-18R, are also elevated in IBD biopsies and can mediate epithelial damage responses.⁷ Epithelial integrity is also regulated by other cell surface protein-protein interactions, such as secreted DAMPs and their corresponding receptors (e.g. HMGB1/RAGE)⁸ and adhesion interactions (e.g. integrins, cadherins and tight junction proteins).^{9,10} Moreover, crosstalk of these cell surface interactions is also important. For instance, TNF activates TNFR2 and induces redistribution of adhesion proteins to

basolateral membranes of intestinal epithelial cells¹¹, while IL-13-induced damage of intestinal epithelial cells requires TWEAK and its receptor (Fn14).¹²

While a broad spectrum of IBD-omic studies look for disease relevant genes at the individual level, assessment of co-ordinately regulated ligand-receptor pairs is still lacking. To address this question, we developed a Protein-Protein Interaction (PPI)-guided IBD meta-analysis with a specific focus on cell surface and extracellular proteins, aiming to uncover novel IBD-associated ligand-receptor pairs, followed by functional investigations in the intestinal epithelium. Among the identified ligand-receptor pairs, urokinase-type Plasminogen Activator (uPA, *PLAU*) and its receptor (uPAR, *PLAUR*) both display significant expression increase in IBD biopsies, leading us to investigate their potential roles in IBD pathogenesis.

The uPA-uPAR system has been implicated in a variety of cellular activities, including cell proliferation, adhesion, invasion and survival.¹³ The serine protease uPA cleaves and activates plasminogen, which triggers a proteolytic cascade to modulate extracellular matrix (ECM) proteins. Activation of uPA from pro-uPA is enhanced by the interaction with its receptor uPAR.¹⁴ The receptor, uPAR, is also involved in various intracellular signalling pathways through interaction with other cell surface proteins, including integrin subunits, GPCRs and EGFR. These interactions activate diverse signalling pathways including ERK, AKT and PI3K.¹³

In this study, we identified a coordinated regulation of uPAR and uPA in the IBD mucosa and during barrier breakdown of primary human intestinal organoids. We investigated the uPA-uPAR pathway in the regulation of intestinal barrier integrity *in vitro* with primary intestinal organoid-derived monolayers, and *in vivo* using the Dextran Sulfate Sodium (DSS)-induced colitis model. Our results demonstrate a key role of the uPA-uPAR interaction in the epithelial barrier and highlight its therapeutic potential for IBD mucosal healing.

Methods

Ethics

Primary human intestinal organoids were generated from primary small intestinal tissues obtained from Conversant Bio (now Discovery Life Science, DLS), which has Institutional Review Board/Ethics Committee (IRB/EC) processes that dictate the procedure for actions such as submission and amendment of protocols, obtaining applicable approvals and informed consent from participants. For the primary human intestinal tissues used in our study, DLS has obtained IRB/EC approval and the consent of the participants/donors. DLS procures tissues for research from post-mortem sites, such as Organ Procurement Organizations (OPO) sources under next-of-kin consent forms.

The tissues obtained from DLS fulfil all Boehringer Ingelheim (BI) legal, ethical, and regulatory requirements.

In vivo studies were conducted in compliance with the rules set forth by the BI site Institutional Animal Use and Care Committee (IACUC) and in accordance with the guidelines established in the National Institutes of Health, Guide for the Care and Use of Laboratory Animals. All protocols were reviewed and approved by the site's IACUC. *In vivo* studies were conducted at a BI facility that was accredited by the International Association for the Assessment and Accreditation of Laboratory Animal Care (AAALAC) accredited facilities. Euthanasia was performed in accordance with the guidelines established in the Panel on Euthanasia of the American Veterinary Medical Association. All mice were housed under 12 h light/dark cycles with free access to food and water. Experimentation was conducted with consideration to minimize animals' pain and distress.

IBD meta-analysis

The IBD meta-analysis was performed with 15 published IBD studies (Table S1), including RNA-seq and micro-array datasets with a total of 1020 IBD tissue samples (UC or CD) and 373 controls. To better represent the disease condition for meta-analyses, we selected the disease group for comparison based on the categorization defined in each study. In general, our selection criteria include: 1) If disease samples include inflamed and non-inflamed tissues, we used samples from inflamed tissues as the disease group (2 studies: E-MTAB-5464; GSE57945); 2) If disease samples include any treatment, we used samples prior to treatment as the disease group (4 studies: GSE10616; GSE16879*; GSE73661; GSE52746); and 3) If disease samples include active and inactive patients, we used samples from active patients as the disease group (4 studies: GSE59071; GSE75214; GSE52746; GSE37283) (see supplemental information and tables for details). Microarray studies were processed with R Affy package and quantile normalization was applied to adjust between array baseline biases. NGS datasets were mapped to human reference genome GRCh37.75 using STAR alignment (v 2.5.2b). Gene counts matrix was later generated using featureCounts tool from Subread package (v 1.6.0).

Differentially expressed gene significance between disease patients (UC or CD) and healthy controls from each study was obtained using GLM model from R limma package (v. 3.1) (for micro-array datasets) or R package DESeq2 (v. 1.6.3) (for RNA-seq). Overall significant genes were determined through a slightly modified *r*-th ordered *p* value approach.¹⁵ We selected genes with fold change ≥ 1.5 and adjusted *p* value ≤ 0.05 for subsequent analysis.

We intersected the significantly upregulated genes with a pool of 7 PPI databases: Intact (v4.2.12)¹⁶, HIP-PIE (v2.2)¹⁷, PIPs (v 12/09/2008)¹⁸, BioGrid (v3.5.178)¹⁹, Intomics® (v 2018)²⁰, Clarivate Analytics MetaCore® (v4.2.3) (<https://clarivate.com/cortellis/solutions/early-research-intelligence-solutions/>) and CellphoneDB (v2.0.0.0).²¹ A majority voting mechanism was applied to select high-confidence ligand-receptor pairs. Candidates with ≥ 4 PPI databases support are defined as high-confidence pairs, since they are identified by more than half of the PPI databases used (4 out of 7). Table S2 includes detailed information of the 18 candidate pairs identified in this approach.

Primary intestinal organoids isolation and culture

Isolation and culture of primary intestinal organoids was performed as previously described.^{22,23} Briefly, human small intestinal tissues (obtained from Coverant Bio, now Discovery Life Sciences, <https://www.dls.com/biospecimens/>) were resected from donors and dissected to recover the epithelial mucosa. Murine small intestinal tissues were isolated in house. Epithelial crypts were isolated using EDTA chelation and centrifugation. Crypts were embedded in 3-D Matrigel (Corning #354230) droplets. Culture media for primary human or mouse organoids are listed in Table S4. Organoids were passaged regularly using Cell Recovery Solution (Corning #354253). During each passage, organoids were broken up into smaller pieces by pipetting thoroughly in Cell Recovery Solution before seeding to a new plate. Only organoids less than 80 days in culture were used in this work.

Cells and reagents

Caco-2 cells (ATCC HTB-37) were purchased from American Type Culture Collection (ATCC) and authenticated by Short Tandem Repeat (STR) profiling according to the cell bank. Mycoplasma was tested in house. Caco-2 cells were cultured in Dulbecco's Modified Eagle Medium (DMEM) with heat-inactivated Fetal Bovine Serum (FBS). Cells were passaged every 3-4 days with 0.25% Trypsin-EDTA at the ratio of 1:5–1:8. Dharmacon Accell siRNA targeting uPAR, uPA or non-targeting control siRNAs were listed in Table S4. siRNA delivery followed Dharmacon Accell siRNA protocols. In monolayer assay with siRNA treatment, cells were treated with 1 μ M siRNA 3 days prior cytokine stimulation. Plasmids expressing uPAR, uPA and control plasmids were purchased from OriGene (#RC201222, #RC202083 and #PS100001). Fugene 6 reagent was used for plasmid transfection.

All antibodies and TaqMan probes included in this study are commercially available and the Research Resource Identifiers (RRIDs) are listed in Table S4. Recombinant human or mouse TNF- α and IFN- γ were purchased from Humanzyme (#HZ-1014) and R&D

systems (#285-IF-100/CF; #410-MT/CF; #485-MI/CF). Cytokines were added at a concentration of 10 ng/ml. In the experiments with EGF treatment, the final concentration of EGF (Life Technologies, #PHG0311Z) was 50 ng/ml.

Small molecule inhibitors (IPR-1110 and WX-UK1) and small peptide inhibitor (AE234 and AE147) were described previously.^{24–27} Antibody ab5329 was purchased from Novus Biologicals (#H00005329-B01P). In experiments with inhibitor treatment, working stocks (1000x in DMSO; 3 mM or 10 mM) were diluted in DMSO following a step-wise dilution method to a final concentration of 3 μ M or 10 μ M. A corresponding amount of DMSO was diluted in the same fashion and was used as control treatment. In experiments with antibody treatment, antibody stock (1 mg/ml) or mouse IgG control (same concentration) was diluted in sterile endotoxin-free water to a final concentration of 15 μ g/ml. In experiments with small peptide treatment, the working stock (1000x in water; 3 mM) was diluted in sterile endotoxin-free water to a final concentration of 3 μ M. A corresponding amount of water was used as control treatment. uPAR and uPA CRISPR KO pool cells were generated by the Genome Engineering and iPSC Centre (GEIC) at Washington University in St. Louis. Approximately 1×10^6 single cells were washed in DPBS and resuspended in P3 primary buffer (Lonza) with gRNA/Cas9 ribonuclease protein (RNP) complex (200 pmol gRNA + 80 pmol SpCas9) and then electroporated with a 4D-Nucleofector (Lonza) using CA-137 program. Following nucleofection, cells were screened with targeted deep sequencing analysis using primer sets specific to target regions. gRNA sequences were listed in Table S4. KO pool cells at passage 1–3 were used in this work.

Cell growth and apoptosis analyses were performed using an IncuCyte S3 Live Cell Imaging system. The IncuCyte® Caspase-3/7 and Annexin V Dyes were used to detect apoptotic cells. Data analysis was performed with the IncuCyte software and GraphPad Prism.

Monolayer assay

Dense and rapidly growing organoid cultures are important for successful monolayer assays. One full grown 24-well plate of 3D organoid culture (Figure 2a as an example of full-grown organoid culture) was used to seed one 24-well transwell plate (Corning #3397). Prior to seeding the transwell plate, the inserts of the transwell plate were coated with 50 μ L Matrigel solution (Corning #354230; 1:40 dilution in DPBS) and incubated at room temperature for at least one hour. During transwell coating, organoids were recovered from 3D Matrigel droplets using Cell Recovery Solution (Corning #354253) and broken into small fragments (around 10 cells) with vigorous pipetting. These organoid fragments were then resuspended in organoid growth media with additional mixing to ensure homogenous

distribution. 0.3 mL organoid fragment-containing media was added to each transwell insert. One insert was added with only growth media and served as blank control for TEER reading. Next, 1.4 mL organoid growth media was added to each outer chamber. The seeded transwell plate was shaken well to ensure homogenous distribution of the organoid fragments and kept at room temperature for 10 minutes before transferring to a tissue culture incubator.

In the monolayer assay with Caco-2 cells, Caco-2 cells were collected and counted in triplicates via the use of the Invitrogen Countless Cell Counter. Cells were broken into single cell solution with vigorous pipetting and seeded to the 24-well transwell at a concentration of 0.1×10^6 cells per insert (0.33 $\times 10^6$ /mL; 0.3 mL/insert). The seeded transwell plate was shaken well to ensure homogenous distribution of the cells and kept at room temperature for 10 min before transferring to the tissue culture incubator.

To induce barrier breakdown, TNF- α and IFN- γ were added to the transwell at a concentration of 10 ng/ml. In experiments with inhibitor treatment, inhibitory molecules were added 30 min before cytokine treatment. TEER levels were monitored every other day. Supernatant from inner wells was collected for ELISA assays. Electronic resistance (ohm) was assessed using an epithelial volt/ohm meter with an STX2 electrode set (World Precision Instruments). TEER values were calculated by the following equation: $TEER = (Ohm_{sample} - Ohm_{control}) \times 0.33 \text{ cm}^2$. Pre-barrier formation samples were collected 24 h after transwell seeding. Post-barrier formation time points were determined when the increase of TEER values reach a plateau. Barrier breakdown samples were collected when TEER values reduces 70% or more (2–3 days after cytokine treatment).

FITC-Dextran molecules were used for permeability assessment for Caco-2- and primary organoid-derived monolayers. 10000 (MW) FITC-Dextran was used in Caco-2 permeability assays and 4000 (MW) in primary-organoid derived monolayers. Briefly, FITC-Dextran solution was added to the upper chamber of the transwell to a final concentration of 0.5 mg/ml 2 days after cytokine stimulation and incubated for 4 h. Medium from lower chamber was then collected for fluorescein detection via the use of a VICTOR plate reader. Permeability (%) was calculated by normalizing to the read of the control group.

mRNA assessment

Cultured cells were lysed with RLTplus buffer from Qiagen and RNA extraction was performed with a QIAasympy instrument and reagent. Mouse distal colon tissue was homogenized in Trizol and RNA was extracted through phenol-chloroform purification. RNA quality and quantity were measured by Nanodrop.

cDNA was generated using Invitrogen SuperScript Vilo kit (#11754050). Taqman assay was performed using a ViiA 7 instrument. Relative expression was calculated with $\Delta\Delta$ -Ct methods and *GAPDH* (*Gapdh*) was used as normalization control unless otherwise noted. Nanostring analysis was performed according to manufacturer's instructions. Mouse immunology panel (547 target genes + 14 internal reference genes) and fibrosis panels (760 target genes + 10 internal reference genes) were used to profile gene expression in the DSS study. Nanostring results were analysed in nSolver™ software and counts were normalized to internal controls. DSS upregulated genes were defined with fold change over 1.5 ($p < 0.05$) in WT mice after DSS treatment. Protected genes were defined with a lower fold change in the uPAR deficient mice ($p < 0.05$). <http://geneontology.org/>.

Western blot (WES)

Cells were washed with PBS and lysed on ice in RIPA buffer (Pierce #89900) with 1x protease inhibitor cocktail (Roche #4693159001) and 1x PhosSTOP (Roche #4906845001). Protein concentration was measured by BCA protein assay. Protein analysis were performed with the WES™ immunoassay, an automated western-blot platform based on capillary electrophoresis combined with chemi-luminescence. Samples were prepared following the manufacturer's instructions (ProteinSimple) and expression levels were calculated based on the digital peak area intensity using the COMPASS software. α -tubulin was used as a loading control. The full blots of all the WES results (including Immunoprecipitation) are presented in the supplemental file.

ELISA and uPA-uPAR interaction assay

uPA (urokinase) secretion was measured by Quantikine ELISA kits from R&D Systems (#DUPA00). Supernatant from the inner well was collected at the desired time point and diluted 1:2 to 1:5 in PBS for ELISA. The assay was performed following manufacture's manual. Protein levels were calculated based on the standard curve.

In the uPA-uPAR interaction ELISA experiment (Figure 4e), 25 μ l of a 2 μ g/ml uPAR solution was coated to Maxisorp ELISA plates (Nunc #464718) at room temperature for 1 h. Plates were washed 4 times with 0.05% Tween-20 solution and subsequently blocked with 5% BSA in PBS at room temperature for 1 h. Then the antibody was titrated at concentrations ranging from 0.3–250 nM in the presence of 10 nM uPA and incubated over night at 4 °C. Plates were washed 4 times with 0.05% Tween-20 solution. Binding levels of uPA were detected with an HRP-labelled (horseradish peroxidase) anti-human uPA polyclonal rabbit antibody (Molecular Innovations #ASHUPA-GF-HRP). The detection antibody was used at 1.26 μ g/ml

and incubated at room temperature in the absence of light for 1 h. Plates were subsequently washed 4 times with 0.05% Tween-20 solution. TMB (3,3',5,5'-tetramethylbenzidine) was added as a substrate for HRP and the reaction was stopped with 1M HCl after incubation for 7 min. Data was recorded on an ELISA reader at 450 nm and referenced to the signal at 620 nm. IC₅₀ of the ab5329 antibody was determined in GraphPad Prism using a 4-parameter fit.

Immunoprecipitation (IP)

30–50 μ l Dynabeads Protein G (ThermoFisher) was first incubated with 1 μ g antibody against target protein or rabbit IgG control for 1 hour at room temperature, followed by an overnight incubation with 1mg protein lysate at 4 °C. On the next day beads were collected using a magnetic stand and the “unbound” samples were collected to check IP efficiency. Beads were washed with cold IP lysis buffer and eluted with low-PH elution followed by neutralizing reagent buffer (Pierce #88804). Protein levels in IP complex were assessed by western blot (WES). Both uPAR IP (IP with uPAR antibody and blot with integrin subunits and EGFR antibodies) and the corresponding reciprocal IPs (IP with integrin subunits or EGFR antibody and blot with uPAR antibody) were included. Protein levels in the input samples (cell lysates prior to beads incubation) were also evaluated.

Phospho-protein profiling

Protein phosphorylation profiling was performed following the instructions from R&D Systems. Cell lysates were prepared using lysis buffer provided in the kit. 400 μ g cellular protein was used for each assay. Dot blot signal intensity was analysed using ImageJ. Average intensity of the duplicates was used for data analysis. Relative intensity was analysed by subtracting the negative control first, followed by normalization using reference spot (positive control). Fold change after stimulation was calculated using the relative intensity.

Immunofluorescence and microscopy

For immunofluorescent staining, cells were grown in a monolayer, washed in cold PBS and fixed with 4% paraformaldehyde. Fixed cells were directly blocked with PBS + 0.2% Triton X-100 + 10% Donkey Serum (Jackson Laboratory). Mouse distal colons were fixed in 10% formalin and cut into 4 μ m sections. The sections were dewaxed, rehydrated and subjected to heat-induced epitope retrieval with Retrieval Solution 1 on a Leica BOND III, before blocking with Dako Protein Block (Serum-free). The samples were incubated with primary antibody overnight at 4 °C. Anti-uPAR (RD System #AF807) Ab and anti-JAM-A Ab (Bethyl Laboratories #A302-891A) were used at a concentration of 1:200;

anti-ZO-1 Ab (Abcam #ab216880) was used at a concentration of at 1:400. The next day, cells were washed and incubated with corresponding secondary antibodies (Jackson Laboratory, 1:800) and DAPI (Invitrogen). Immunofluorescent images were taken with a ZEISS LSM880 Confocal Microscope. Bright field 3D organoid images were taken with a ZEISS Axio Observer Inverted Phase Contrast Microscope. Bright field 2D monolayer images were taken with an IncuCyte S3.

DSS-induced colitis in mice

Mice with the C57BL/6 background were used in this study. The uPAR KO (*Plaur* ^{-/-}) mice²⁸ and wildtype (WT) littermates were purchased from Jackson Laboratory (strain number #002829). Colitis was induced in 9–10-week-old age-matched WT ($n = 17$) and uPAR KO mice ($n = 18$) using 5% DSS [Dextran Sulfate Sodium salt, colitis grade (36,000–50,000), MP Biomedicals, LLC] provided for 5 days in the drinking water, followed by normal drinking water for 2 days. WT mice fed with normal drinking water served as the naïve group ($n = 8$). The WT mice were randomised into treatment arms (naïve or DSS-treated). During DSS treatment, body weight was measured daily. At the end of the experiment, mice were sacrificed on day 7 and their colon was removed, weighed and measured to determine colon weight to length ratio. Distal colon samples were collected immediately for RNA isolation and histological analysis.

Histological analysis

Distal Colons were fixed in 10% formalin and stained with routine H&E. Histology was scored in a blinded fashion as described previously.²⁹ Briefly, histology scores include a combination of epithelium morphology change (score 0–4; same below), inflammatory cell infiltration/inflammation and mucosal ulceration. Score 1–4 indicated that the damage was observed in <25%; 25–50%; 50–75% and 75% area, respectively, while score 0 indicated normal condition. A total number of four H&E sections per animal were assessed for each sample and the average scores were used. Finally, the sum scores were determined by the combined numbers of all three parameters, representing the overall histopathology status of each sample. Representative images were acquired with a Leica AT2 digital scanner. Histology images with a score close to group average were displayed as examples.

Statistical Analysis

In all bench experiments presented, three or more biological replicates were included for statistical analysis. All data were shown as mean \pm SD in the figures. Shapiro-Wilk Test was used to verify the assumption of normality. Student *t* test or ANOVA analysis was

performed for datasets passed Shapiro-Wilk Test ($\alpha = 0.05$). Non-parametric test was used for datasets failed to pass the test (Figure S4 a-i). Statistical analysis was performed using Prism GraphPad Software. *p* values are labelled in the figure. For the transcriptome meta-analysis, the statistical methods (*r*-th ordered *p* value approach) were described above.

Role of funding source

The study was funded by Boehringer Ingelheim and all authors were Boehringer Ingelheim employees during the study.

Results

Ligand-receptor transcriptome meta-analysis identifies uPA-uPAR as a co-regulated pair in IBD

With the advances in bioinformatic algorithms and growing gene expression databases in the public, it is possible to generate new hypotheses through investigating co-regulation of functional gene pairs in disease. Here we report a comprehensive meta-analysis approach aimed at identifying IBD associated ligand-receptor pairs by integrating cell surface PPI databases. As listed in Figure 1a, we selected fifteen IBD datasets from public sources (six Ulcerative Colitis, two Crohn's Disease and seven combined studies), including a total number of 1020 IBD tissue samples (UC or CD) and 373 controls. We followed the disease and control groups exactly as defined in the original publications and a full description is available in the Methods, Table S1 and S5. We constructed detailed comparisons by subsets and biopsy locations, and applied *R*-th ordered *p* value (rOP) ranked algorithm¹⁵ to leverage result from each individual comparison to derive a final aggregated significance for each gene. We next queried the significantly regulated genes over seven PPI databases with a specific focus on interactions between cell surface proteins and extracellular proteins for ligand-receptor identification (Figure 1a, see supplemental methods for details). A majority voting mechanism was then applied to select high confidence ligand-receptor pairs. Around 130 candidate pairs were identified with significant upregulation of both receptor and ligand in disease groups (median fold change ≥ 1.5 ; adjusted $p \leq 0.05$). Among them, a total number of 18 high-confidence gene pairs were further selected with four or more supporting PPI databases (Table S2). We focused on non-chemokine genes to explore novel IBD-associated ligand-receptor pairs (Figure 1a). We found several previously reported IBD risk genes or pairs, thus validating our meta-analysis approach. For example, Oncostatin M and its receptor (OSM-OSMR) have been reported to drive intestinal inflammation, serving as both biomarkers and therapeutic targets for IBD.³⁰ ICAM1 (also known as LFA1) has also been identified as potential

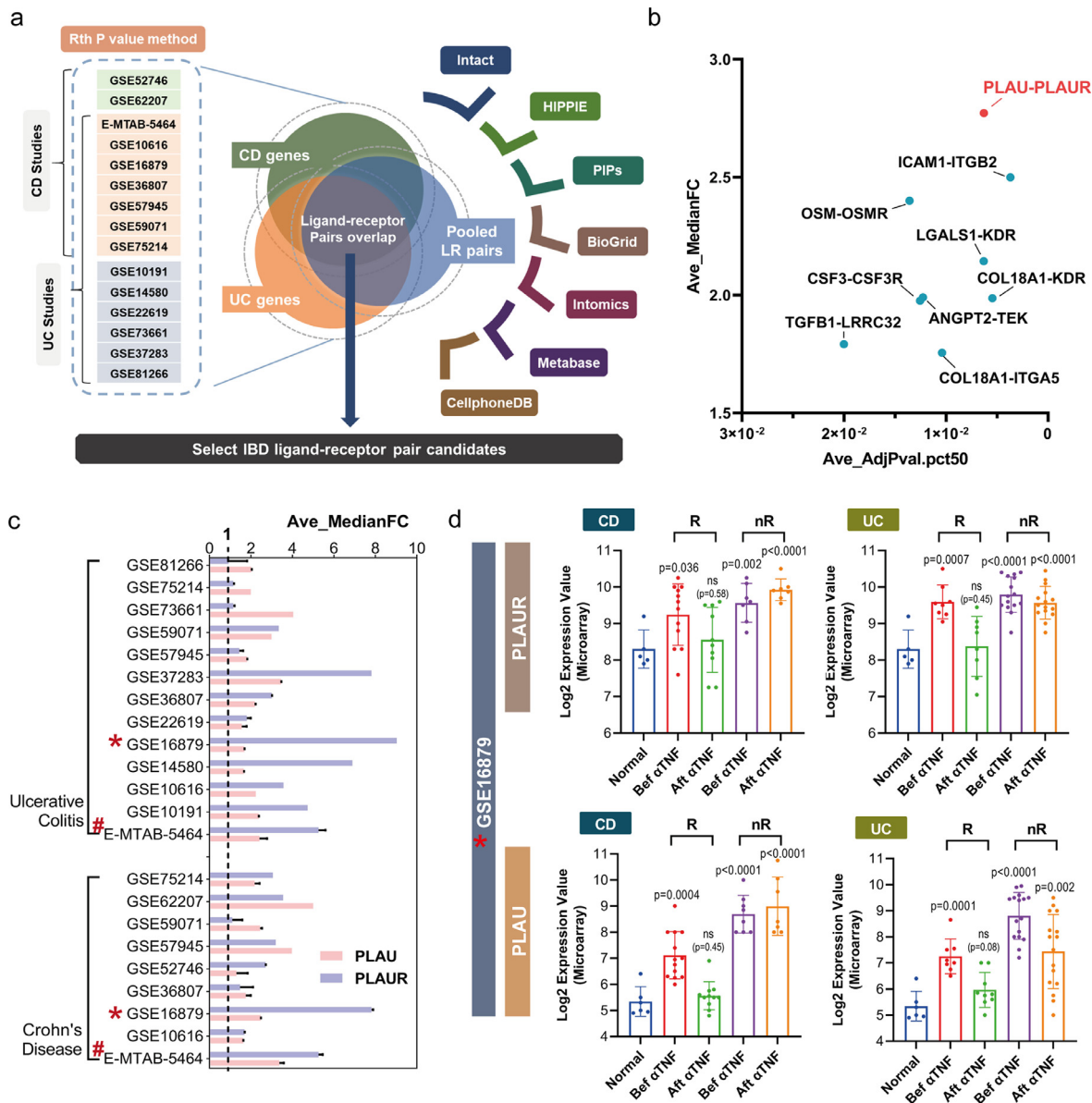


Figure 1. The search of co-regulated ligand-receptor pairs in IBD mucosa. (a). Meta-analysis on 15 human IBD studies was performed and aggregated p value (after BH correction) for each gene was obtained by r-th ordered p value approach for UC and CD subtypes: specifically, 50 percentile p value was used to represent final p value of a given gene in either CD or UC group compared to normal. Significantly up-regulated genes were selected based on a cut-off final p value < 0.05 and median fold change > 1.5. Separately, an internal ligand-receptor pool (See Methods) was established based on surveying Protein-Protein-Interaction (PPI) databases. Ligand-receptor relationship was defined by intrinsic algorithm of the databases. The overlap of CD and UC significant genes from meta-analysis was further intersected with the ligand-receptor pool. High-confidence IBD ligand-receptor pairs were selected with 4 or more supporting PPI databases. (b). Ligand receptor pairs identified from the workflow above. Average values of the pair (FC and adjusted p) were used in the plot. Note that chemokines and receptors were removed from the graph to highlight the other pairs. See a full list in Table S1. (c). Expression of uPAR and uPA in all the studies examined. Median fold change between IBD and normal samples was used to assess the induction. GSE16879 (highlighted with *) was displayed in Figure 1d (anti-TNF study). E-MTAB-5464 (highlighted with #) was displayed in Figure S1 (IBD epithelial cell study). (d). mRNA levels of uPAR and uPA in UC and CD responder/non-responder patients, before and after treatment of anti-TNF (infliximab), compared with non-IBD controls. (GSE16879).³² R., anti-TNF responders; nR., anti-TNF non-responders; Bef *α*TNF, before anti-TNF treatment; Aft *α*TNF, after anti-TNF treatment. All data are shown as mean ± SD and are analysed using 1-way ANOVA followed by Dunnett’s multiple comparison test. ns, non-significant.

targets for IBD treatment, although results from clinical studies with anti-sense oligonucleotides are inconclusive.³¹

Of all the pairs, uPA-uPAR (PLAU-PLAUR) stood out as a top ligand-receptor candidate pair with high median fold change and low adjusted p values, indicating a strong link with IBD (Figure 1b, red). A comprehensive analysis of uPAR and uPA expression across the studies (Figure 1c) showed that the pair is co-ordinately upregulated in both UC and CD patients. Interestingly, we found that both uPAR and uPA showed higher expression in α TNF (Infliximab) non-responders, compared to responders after α TNF treatment (Figure 1d, GSE16879).³²

We noticed that one study included in the meta-analysis (E-MTAB-5464)³³ focused on intestinal epithelial cells from IBD patients and a significant induction of uPAR and uPA was shown by our meta-analysis (Figure 1c). Further analysis of the Howell study³³ showed that uPAR and uPA are co-ordinately increased in CD and UC epithelial cells isolated from different sections of the intestine (Figure S1a). The expression levels also correlate with the inflammation status according to the diagnostic histopathology scores (Figure S1a-b). These findings indicate a potential role of uPAR and uPA in regulating intestinal epithelial cells in IBD.

Expression of uPAR and uPA negatively correlates with intestinal barrier integrity

To understand the roles of uPAR and uPA in intestinal epithelial regulation, we first assessed the expression of uPAR and uPA in a primary human intestinal organoid-derived monolayer assay. A human intestinal epithelial organoid (“epithelial mini-guts”) *in vitro* culture system was generated using crypts of healthy small intestine donors as previously described.²² We further developed primary organoid-derived monolayer assays to enable functional studies, as illustrated in Figure 2a. In all four primary organoid donors we observed an increase in TEER values over time, indicating the formation of an intact barrier. To trigger barrier breakdown, we challenged the barrier simultaneously with IFN- γ and TNF- α ⁷ and observed a reduction of barrier integrity in all four donors (Figure 2b).

Expression of uPAR and uPA increased at both mRNA and protein levels after cytokine-induced barrier breakdown (Figure 2c). This result is consistent with the discoveries from the ligand-receptor IBD meta-analyses that uPAR and uPA are co-ordinately regulated in IBD (Figure 1 and Figure S1). Interestingly, we also observed a significant reduction of uPAR and uPA expression during barrier formation in all four donors (Figure 2c). Such inverse correlation between uPA-uPAR expression and barrier integrity strongly implies a role of uPA-uPAR in regulating epithelial barrier

integrity and that induced expression of uPAR and uPA may enhance barrier breakdown.

Epithelial cells deficient of uPAR or uPA are more resistant to barrier damage and display enhanced barrier formation

We next investigated whether genetic deletion of uPAR or uPA protects intestinal epithelial cells from cytokine-induced barrier disruption. Due to technical challenges of genetic interventions in primary intestinal organoids (low and unstable transfection efficiency), we investigated uPAR and uPA expression and function in human Caco-2 cells, a well-studied cell model for intestinal barrier function. Consistent with the observations in organoid-derived monolayers, TNF- α and IFN- γ triggered breakdown of the Caco-2 barrier and the expression of both uPAR and uPA was induced during this breakdown (Figure 3a, parental groups). We next generated Caco-2 CRISPR-KO cell pool targeting uPAR or uPA (Figure 3a). Monolayers derived from uPAR or uPA-deficient Caco-2 cells were more resistant to cytokine-induced barrier damage as assessed by TEER and FITC-dextran permeability (Figure 3b). In addition, induction of Guanylate-binding protein-1 (GBP1), a protein localized at tight junctions of intestinal epithelial cells in response to IFN- γ ³⁴, was also decreased in the uPAR- or uPA-deficient cells (Figure 3c). Knocking-down uPAR or uPA in Caco-2 cells via multiple siRNAs also resulted in a protective effect (Figure S2a-d).

Maintenance of barrier function is dependent upon coordinated proliferation and cell death, as well as the paracellular integrity determined by tight junctions.¹⁰ To further understand the role of uPAR and uPA in barrier regulation, we next asked if uPAR or uPA deficiency leads to altered cellular activities. Caco-2 uPAR or uPA KO cells displayed no change in proliferation rate as compared to the parental controls during barrier formation (Figure S3a) but showed less cell death after cytokine-induced barrier damage (Figure S3c). We also evaluated the tight junction proteins Zonula occludens-1 (ZO-1) and Junctional adhesion molecule A (JAM-A) during barrier formation and breakdown. We observed that the integrity of tight junction structure (Figure 3e-f, Figure S6a and d) correlates with barrier function as measured by TEER and permeability (Figure 3b). Importantly, barrier damage-associated disruption of tight junctions (as measured by expression of ZO-1 and JAM-A) was markedly alleviated in uPAR or uPA KO cells (Figure 3e-f). These findings indicate that deletion of uPAR or uPA leads to improved resistance to cytokine-induced barrier damage, including resistance to disruption of tight junctions and epithelial cell death, which together contribute to the observed improvement in barrier integrity (Figure 3b).

Next, we asked whether inhibition of uPAR and uPA can improve barrier formation. Caco-2 uPAR or uPA

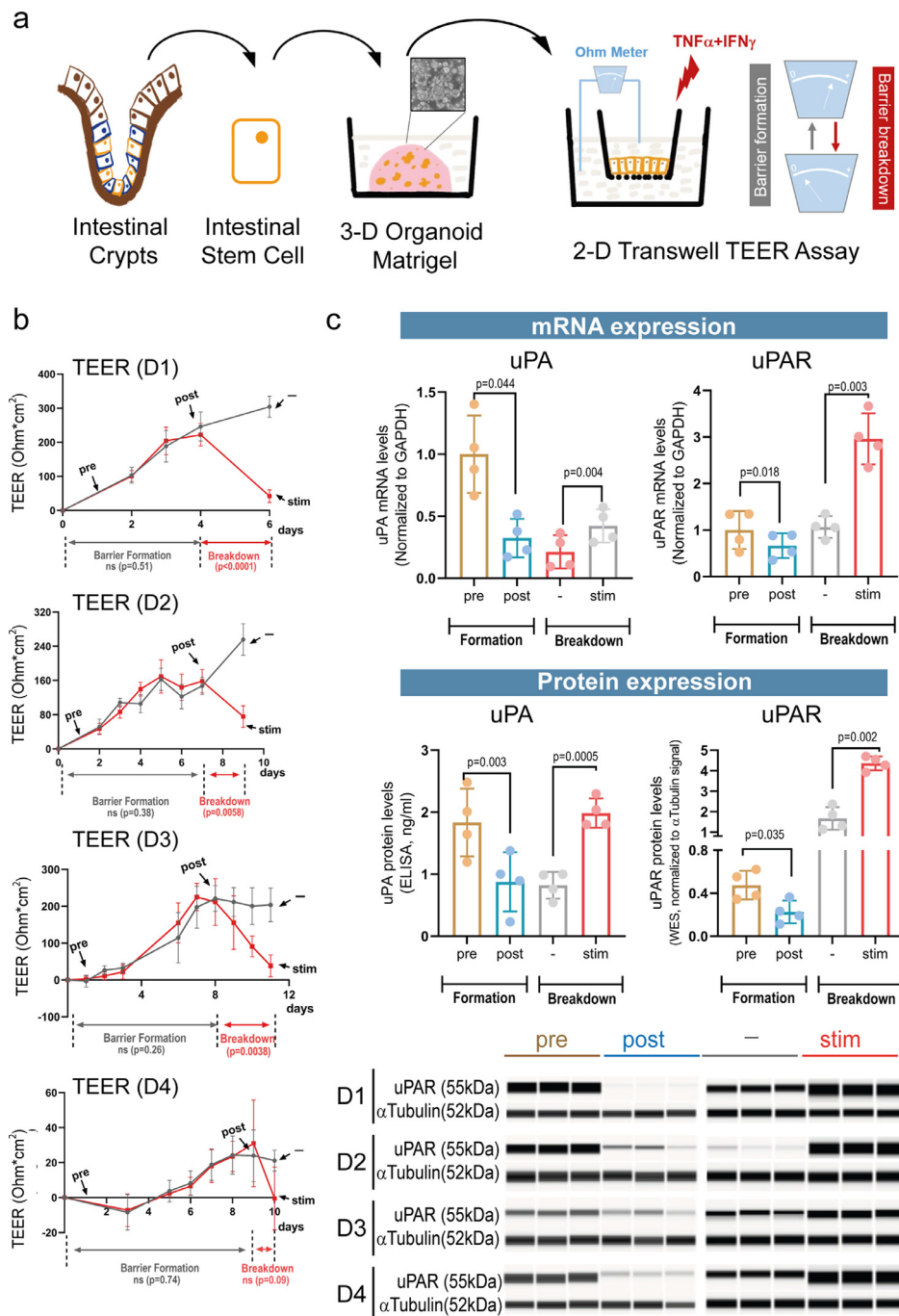


Figure 2. Both uPAR and uPA are upregulated during intestinal epithelial barrier breakdown. (a). Workflow of the monolayer assay derived from primary human intestinal organoids from small intestine (See Methods for details). Monolayer breakdown is triggered by simultaneous $TNF-\alpha$ and $IFN-\gamma$ treatment. (b). TEER assay with four primary intestinal organoid donors (D1, D2, D3 and D4, $n = 20$ /donor, 10 in control and 10 in stim group). For each donor, comparisons between the control and the stim groups during barrier formation and barrier breakdown are shown. Samples at four time points are used for the later studies: pre indicates pre-barrier formation; post indicates post-barrier formation; - indicates control treatment; and stim indicates $TNF-\alpha$ and $IFN-\gamma$ treatment. (c). Relative expression levels of uPAR and uPA during barrier formation and breakdown in four donors ($n = 3$ per donor per condition, repeated 3 times). mRNA levels were assessed by Taqman assay and protein levels by ELISA (uPA) or western blot (uPAR). Protein expression of uPAR was quantified by digital peak intensity values generated by the ProteinSimple COMPASS software and was normalized to the corresponding α -Tubulin peak. All data are shown as mean \pm SD and are analysed using 2-way ANOVA (b) or paired Student's *t* test (c).

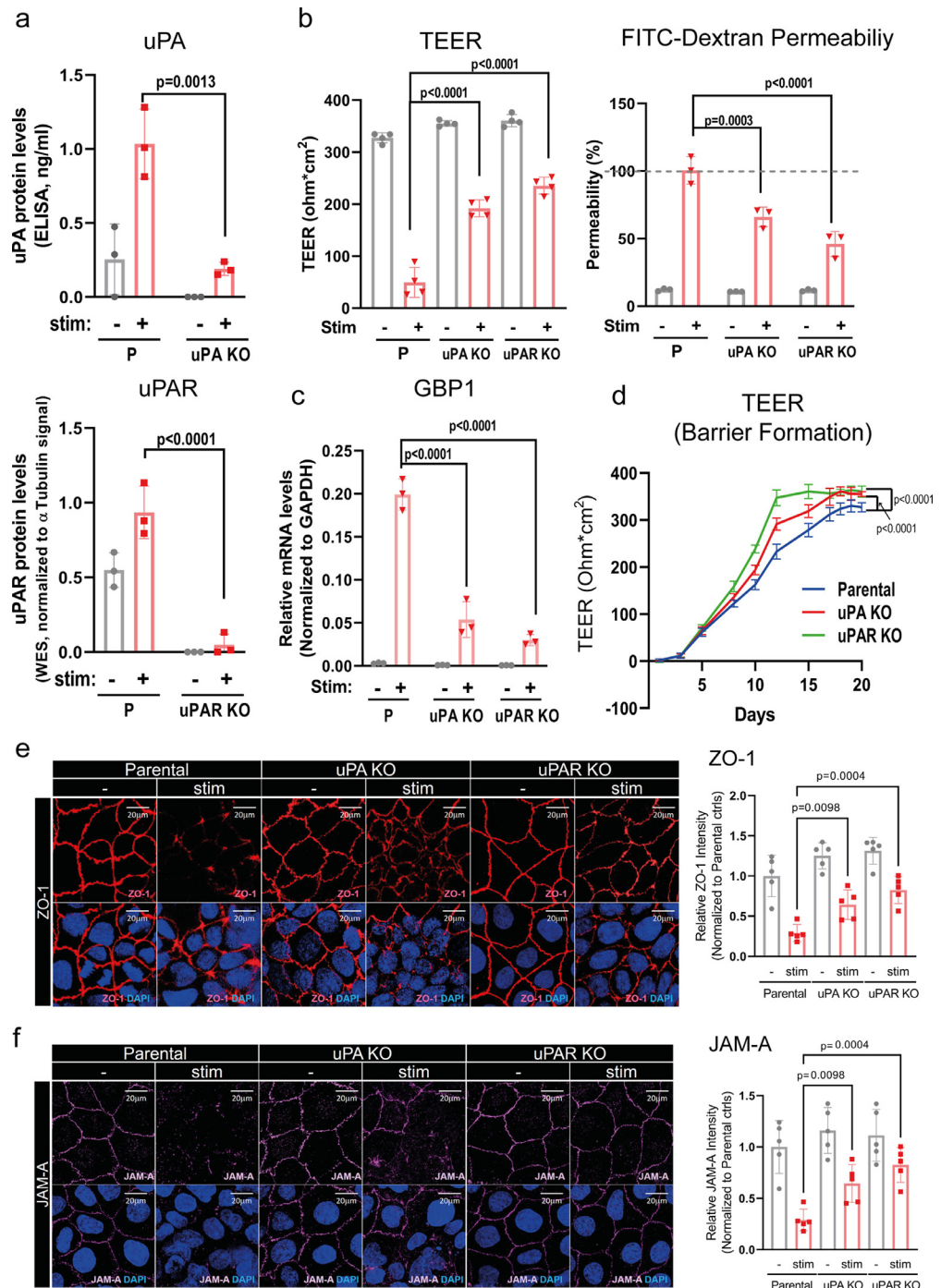


Figure 3. Genetic deletion of uPAR or uPA protects epithelial barrier from cytokine-induced damage. (a). Protein levels of uPAR and uPA in parental and KO cells ($n = 3$ /group, same below). Alternative genetic inhibition assay with siRNAs were presented in Figure S2. (b). Barrier function of uPAR KO cells and uPA KO cells comparing to parental cells assessed by TEER and FITC-Dextran permeability. Permeability (%) is achieved by normalizing to the level of parental cells after stimulation. (c). GBP1 mRNA expression (by Taqman assay) in parental and KO cells. (d). Barrier formation in uPAR and uPA KO cells ($n = 6$ /group). TEER values during barrier formation are shown. (e-f). Localization of tight junction proteins ZO-1 (red) (e) and JAM-A (magenta) (f) in the parental and KO cells before (-) and after barrier damage (stim). Nuclei are visualized with DAPI (blue). Relative intensity is presented on the right ($n = 5$ /group, normalized to parental controls). All data are shown as mean \pm SD and are analysed using 2-way ANOVA followed by Sidák's multiple comparison test (a-c, e-f) or 1-way ANOVA followed by Dunnett's multiple comparison test (d).

CRISPR KO cells showed enhanced barrier formation compared to the parental controls in the absence of any stimuli (Figure 3d). This result was further validated by re-expressing uPAR or uPA in the corresponding KO cells, in which the enhanced barrier formation was weakened (Figure S2e). These findings, together with the observed reduction of uPAR and uPA during barrier formation (Figure 2c), indicates a role of uPA-uPAR during intestinal barrier formation.

Pharmacological Inhibition of uPA-uPAR interaction protects barrier function

We next explored the effects of pharmacological inhibition of human uPA-uPAR on intestinal epithelial barrier function. The ligand, uPA, is a multi-function protein which has enzymatic activity (serine protease) and protein-protein interaction function (binding to uPAR).¹⁴ WX-UK1 (active component of the prodrug Upamostat/MESUPRON®) is a potent inhibitor of uPA protease activity which is being clinically tested for the treatment of multiple solid tumours.²⁵ On the other hand, various PPI inhibitors have been shown to block the interaction of uPA and uPAR, including uPA peptide-derived antagonists AE234 and AE147, as well as a recently reported small-molecule inhibitor IPR-1110^{24,26,27} (Figure 4a). The inhibitory activity of AE234, AE147 and IPR-1110 in blocking uPA binding to uPAR was validated in house, whereas WX-UK1 does not affect the uPA-uPAR interaction. In addition, we evaluated several commercially available uPAR antibodies and identified a neutralizing antibody, ab5329 (Novus Biologicals), which blocks the binding of uPA to uPAR (Figure 4a, e).

Here we applied these pharmacological inhibitors in the primary organoid-derived monolayer and Caco-2 monolayer platforms to assess the role of uPAR and uPA in epithelial barrier regulation. The uPA protease inhibitor, WX-UK1, failed to inhibit the barrier breakdown in Caco-2 cells and in primary epithelial monolayers, indicating that the protease function of uPA is not mediating cytokine-induced barrier breakdown, as measured by both TEER (Figure 4b) and FITC-Dextran permeability (Figure S4). On the other hand, we observed consistent inhibition of barrier breakdown through different uPA-uPAR interaction blockers in Caco-2 cells and moreover, in organoid-derived monolayers from two donors (Figure 4b-d and Figure S4a-i). Among them, the uPAR antibody ab5329 displayed highest protection (50%-80% improvement compared to control IgG treatment), probably due to its potent inhibition of uPA-uPAR interaction. We also evaluated tight junction proteins ZO-1 and JAM-A during barrier formation and breakdown (Figure S5 and S6). Disruption of tight junctions was limited by uPA-uPAR blockers, such as ab5329 in primary human intestinal organoids (Figure S5 and S6f). In addition, uPA-uPAR

inhibitors also lead to improved barrier formation in primary intestinal organoid-derived monolayers (Figure S4j-m). These results are consistent with our findings in uPAR or uPA KO cells, suggesting a protective effect of intestinal barrier integrity achieved by uPA-uPAR inhibition. The observation with different inhibitors also supported the notion that uPA-uPAR interaction, instead of the protease activity of uPA, is key for therapeutic consideration to promote epithelial barrier function.

Inhibition of uPAR sustained EGFR function in barrier protection

Since the ECM protease activity of uPA is not involved in barrier function as shown above, we next focused on the intracellular activities regulated by the receptor uPAR signalling. It has been reported that uPAR regulates intracellular signals through co-receptors, such as integrin subunits and EGFR.¹³ Using the uPAR immunoprecipitation approach, we found that uPAR interacts with integrin subunits $\alpha 5$, $\beta 1$, $\beta 3$ (ITGA5, ITGB1, ITGB3 respectively), and EGFR in the epithelial cells (Figure 5a). Interestingly, the interaction between uPAR and integrin subunits was lost after cytokine-induced barrier damage, while uPAR-EGFR interaction remained (Figure 5a). The results were further confirmed by reciprocal approaches with antibodies against integrin subunits or EGFR (Figure 5a). The specific interaction was confirmed using uPAR KO cells, or in experiments with control IgG (Figure 5a).

We next found that the pro-repair EGFR signalling in epithelial cells, assessed by pEGFR (Y1068)^{35,36}, was better induced in uPAR deficient cells when challenged by pro-inflammatory cytokines (Figure 5b). Furthermore, while EGF significantly protected WT cells against cytokine-induced barrier damage (Figure 5c) and the correlated GBP-1 expression (Figure 5d), the effect was less pronounced in uPAR deficient cells (Figure 5c-d), indicating a negative regulation of EGF/EGFR signalling by uPAR. Given that uPAR interacts with EGFR under normal and damaged conditions, this result supports a role of uPAR in promoting barrier breakdown of intestinal epithelial cells at least partially by suppressing the EGF/EGFR-dependent pathway.

Further investigation on a total number of 45 kinases/phospho-proteins (R&D Systems, ARY003B) confirmed enhanced EGFR signalling in uPAR KO cells (Figure 5e and Figure S7). A detailed list of phospho-proteins and the corresponding fold change values is available in Supplemental Table S3. Also, mitogen- and stress-activated protein kinase (MSK) and cAMP Response Element-Binding Protein (CREB) activation are significantly increased in the KO cells (Figure 5e and Figure S7). MSK is known to mediate phosphorylation and activation of CREB. MSK-CREB signalling has been linked to the regulation of cell junction and

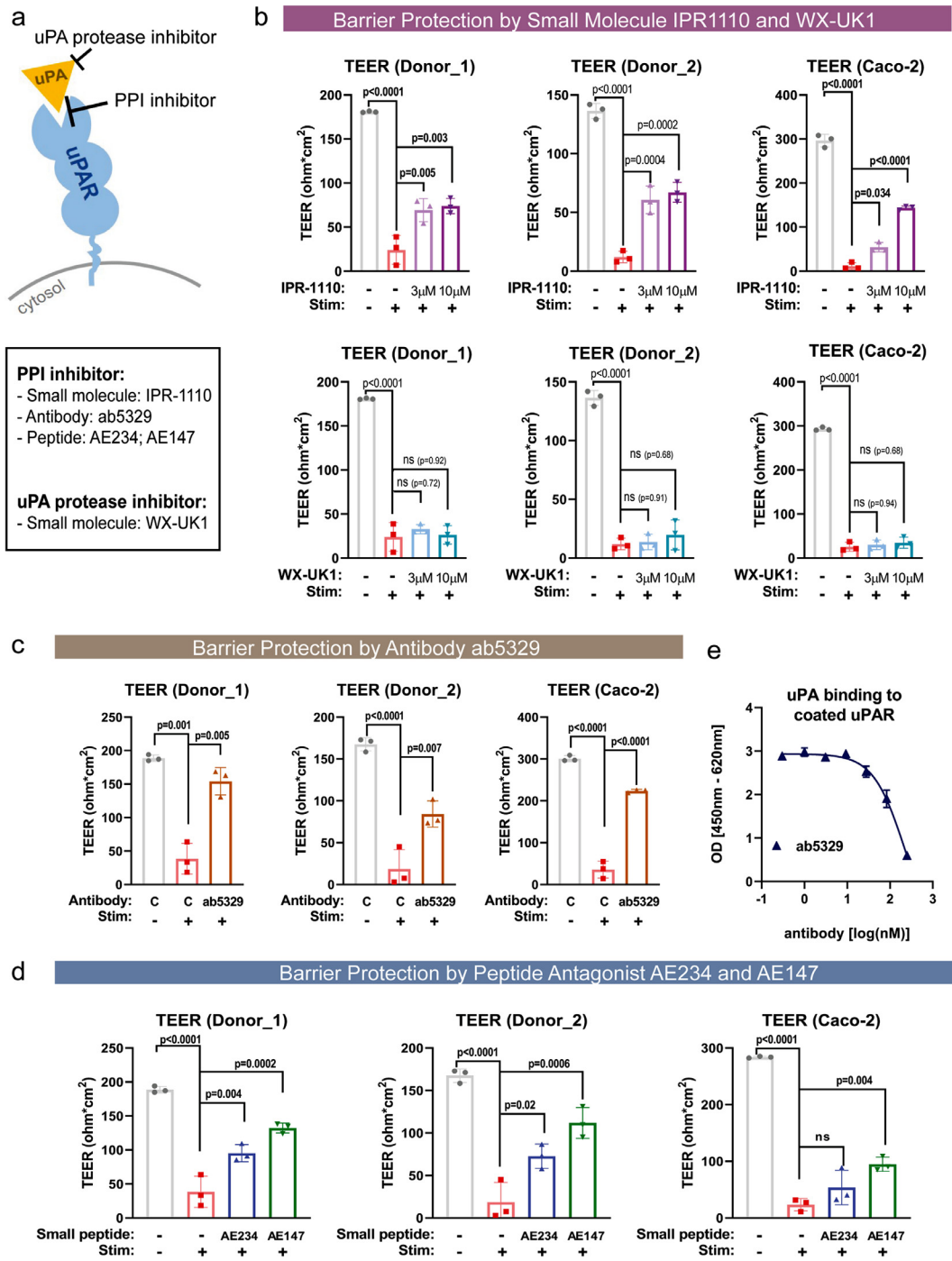


Figure 4. Inhibition of uPA-uPAR interaction through small inhibitors or uPAR antibody protects barrier function in primary organoids and Caco-2 cells measured by TEER. (Equivalent Permeability results are shown in Figure S4) (a). Schematic display of uPA-uPAR inhibition by small molecule inhibitor IPR-1110 and WX-UK1, uPAR antibody ab5329 and small peptide AE234 and AE147. (b-d). Two organoid donors and Caco-2 cells were treated with IPR-1110 and WX-UK1 (b), uPAR antibody ab5329 (c) or small peptide inhibitor AE234 and AE147 (d) during barrier breakdown ($n = 3/\text{group}$). ELISA validation of ab5329 in blocking uPA-uPAR interaction is presented in (e). TEER values after damage are recorded. A corresponding amount of DMSO (0.1%) was used as control for small molecule treatment (b); Mouse IgG at the same concentration was used as control for antibody treatment. All data are shown as mean \pm SD and are analysed using 1-way ANOVA followed by Dunnett's multiple comparison test. ns, non-significant. (e). ab5329 interferes with uPA-uPAR binding by ELISA assay.

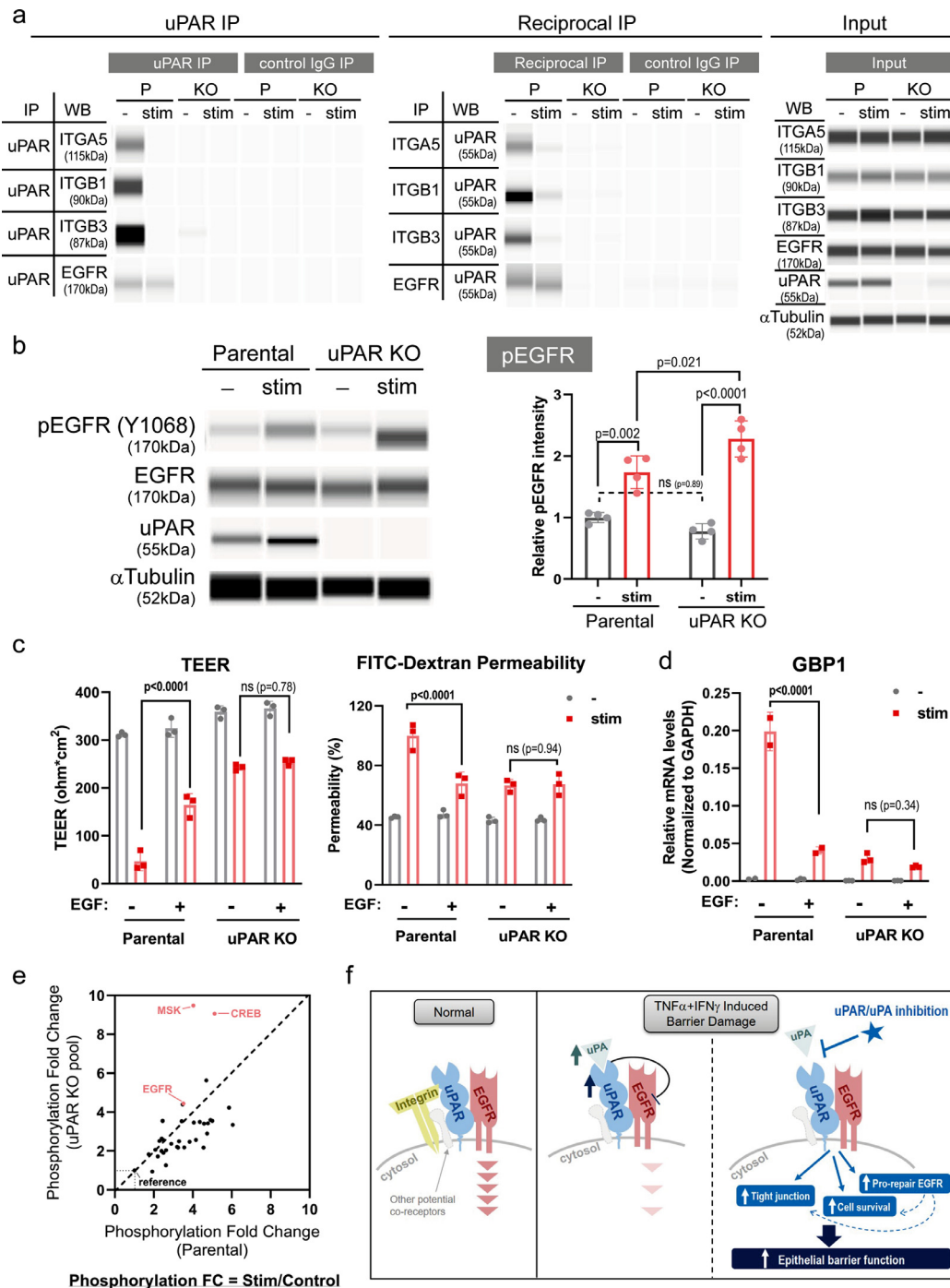


Figure 5. uPAR interacts with EGFR to regulate barrier function. (a). Co-immunoprecipitation (IP) of uPAR and integrin subunit $\alpha 5$, $\beta 1$, $\beta 3$ (ITGA5, ITGB1, ITGB3, respectively) and EGFR. uPAR IP, reciprocal IP and Input were displayed. Stim, TNF- α and IFN- γ treatment for 72 h. P, Parental Caco-2 cells; KO: uPAR KO Caco-2 cells. Both uPAR and the corresponding reciprocal IP were repeated at least 3 times and one representative graph is presented. (b). pEGFR (Y1068) levels in parental and uPAR KO cells after 30 min treatment of TNF- α and IFN- γ . Signal intensity is calculated by 3 replicative experiments (see supplemental file for the full blots of the 3 experiments). (c-d). Parental and uPAR KO cells are treated with EGF followed by barrier breakdown stimulation ($n = 3$ /group). TEER values after breakdown (c) and breakdown-associated GBP1 expression (d) are presented. All data are shown as mean \pm SD and are analysed using 2-way ANOVA followed by Šidák's multiple comparison test. ns, non-significant (b-d). (e). Kinase array from parental and KO cells before and after stimulation. Fold change (FC) of induced phosphorylation in parental and uPAR deficient cells. FC (Stim/Control) is calculated by the signal. Values were adjusted to reference dots. (f). A proposed model for uPA-uPAR in regulating intestinal epithelial barrier.

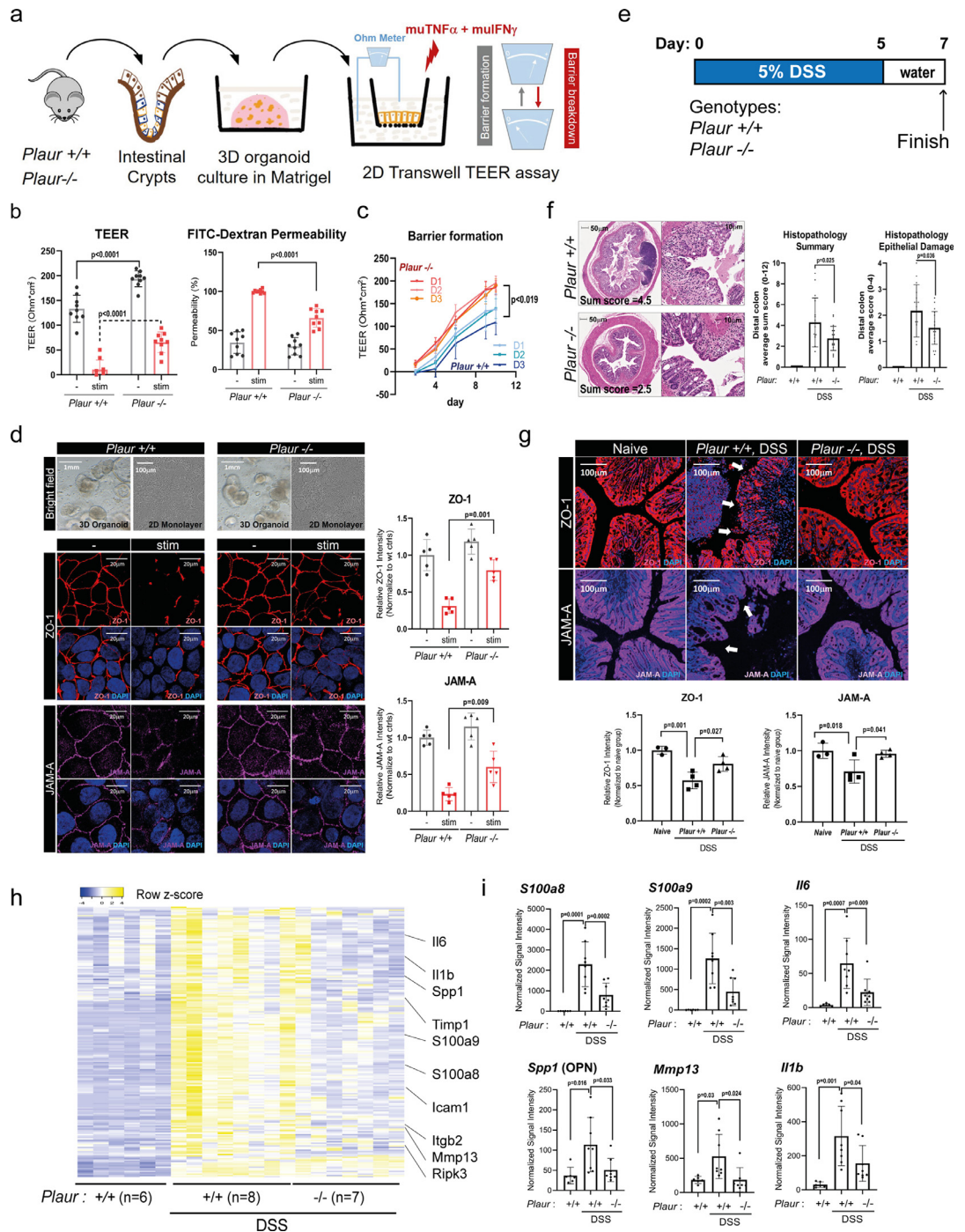


Figure 6. Mice deficient of uPAR display improved intestinal epi-barrier function. (a). Workflow of the monolayer assay derived from primary murine intestinal organoids from WT (*Plaur* ^{+/+}) and uPAR deficient (*Plaur* ^{-/-}) mice. Monolayer breakdown was triggered by simultaneous murine TNF- α and IFN- γ treatment (10 ng/ml each). 3 donors of each genotype were used in the monolayer assay. (b). Barrier function after TNF- α and IFN- γ induced damage in monolayers derived from WT or uPAR deficient murine intestinal organoids (*n* = 9/treatment group). TEER and FITC-Dextran permeability were assessed. Stim, murine TNF- α and IFN- γ treatment for 48 hours. (c). Barrier formation in WT and uPAR deficient monolayers was monitored (3 donors/genotype, D1, D2 and D3). (d). Localization of ZO-1 (red) and JAM-A (magenta) in the murine organoid-derived monolayers before (-) and after (stim) barrier damage. Nuclei are visualized with DAPI (blue) in the bottom panel. Bright field images of 3D organoids and 2D monolayers are presented on the top panel. Relative intensity is presented on the right (*n* = 5/group, normalized to WT controls). ZO-1 and JAM-A protein levels before and after barrier damage are presented in Figure S6e. (e). Workflow of the DSS-colitis study. (f). Histopathology

intestinal permeability³⁷, which also aligns with our findings in the epithelial cells.

Our data suggest the following model (as shown in Figure 5f): During intestinal epithelial damage induced by cytokines, expression of uPAR and uPA is induced. The interaction between uPAR and uPA alters their dynamic interaction with integrin complex and EGFR, which affects the pro-repair EGFR signalling. The epithelial cells display disrupted tight junctions and increased cell death, along with reduced barrier integrity upon the cytokine challenge. Inhibition of uPA-uPAR interaction leads to enhanced EGFR signalling pathway, a reduction in tight junction damage and a reduction in cell death, all of which are reflected in an overall improvement in barrier integrity.

Deletion of uPAR in mice enhances epithelial barrier function *in vitro* and ameliorates epithelial damage in DSS-induced colitis *in vivo*

We next asked if uPAR deficiency could protect intestinal damage in mouse models. We obtained uPAR knock-out (KO) mice from the Jackson Laboratory which have been described previously²⁸ and we confirmed the loss of uPAR at both mRNA and protein levels (Figure S8a). Intestinal organoid cultures were established from WT or KO small intestine and were further adapted into 2D monolayer assays (Figure 6a). Consistent with our previous observations under uPAR inhibition in Caco-2 and human organoid-derived epithelial cells, intestinal monolayers derived from uPAR KO murine intestinal organoids were more resistant to cytokine-induced barrier damage as measured by both TEER and permeability (Figure 6b). In addition, barrier formation was also improved in uPAR KO organoid donors (Figure 6c). Monolayers derived from uPAR deficient organoids displayed improved tight junctions (ZO-1 and JAM-A) (Figure 6d, S6c and e) and reduced cell death after barrier damage (Figure S3b, d), consistent with the observations in barrier function measured by TEER and permeability (Figure 6b). The results recapitulate our findings in Caco-2 cells and primary human organoids.

To further investigate the function of uPAR *in vivo*, we used the Dextran Sulfate Sodium (DSS)-colitis model in WT and uPAR KO mice (Figure 6e).

Expression of uPAR and uPA increased after DSS treatment (Figure S8b). Histo-pathology analysis showed an extensive damage of the colon epithelial structure, crypts loss, surface erosions and inflammatory infiltrate in the lamina propria in WT distal colon after DSS treatment. Notably, uPAR deficient mice displayed significant protection with restored colon mucosa architecture and surface integrity and reduced inflammatory infiltrate, leading to an improvement in histopathology parameters (Figure 6f and Figure S8c). A disruption of tight junctions was observed in WT mice treated with DSS and was significantly reduced in the KOs (Figure 6g), which further indicates a protection of epithelial barrier *in vivo* by uPAR KO. These results are also consistent with the findings of tight junction protection *in vitro* with uPAR deficient mouse organoids (Figure 6d). Although we did not observe a significant difference in overall body weight loss (Figure S8d), the improved colon morphology and reduced epithelial damage in the uPAR KO mice suggests a protective role of uPAR inhibition against DSS-induced colitis.

We next assessed the levels of inflammatory response- and tissue damage-related genes in distal colon tissue from control (naïve) and DSS-treated mice through Nanostring analysis (Mouse Immunology and Fibrosis panels) (Figure 6h-i). Deletion of uPAR alleviated a large number of DSS upregulated genes in DSS-colitis, further confirming the protection of uPAR KO in DSS-induced colitis at the gene expression level (Figure 6h); a full list is available in the supplemental dataset. Many of these genes have been associated with IBD and/or experimental colitis mouse models. For example, S100A8/S100A9, which are subunits of calprotectin, are enriched in the damaged intestine and are clinically relevant biomarkers for IBD.^{8,38} ICAM1 and ITGB2 are both highly associated with IBD pathogenesis³¹ and also showed up in our meta-analysis (Figure 1b). SPP1, or Osteopontin, is another promising biomarker for IBD.³⁹ MMP13, a matrix metalloproteinase, has been linked directly to intestinal epithelial regulation and promotes breakdown of intestinal epithelial barrier integrity in DSS colitis.⁴⁰ IL-6 and IL-1 β are also well-studied cytokines involved in intestinal inflammation and IEC damage in IBD.⁴¹ As illustrated in Figure 6h, an overall >70% reduction was observed in these disease-relevant genes, demonstrating a critical

assessment of naïve WT controls ($n = 8$), WT ($n = 17$) and uPAR deficient mice ($n = 18$) after DSS-induced colitis. 4 sections from each animal were scored in a double-blinded fashion and average scores are presented on the right. See Methods for more details. Representative images were presented with the corresponding scores. (g). Localization of ZO-1 (red) and JAM-A (magenta) in colonic sections from naïve controls, WT or uPAR KO mice after DSS treatment. Nuclei are visualized with DAPI (blue). Regions with disrupted tight junction are marked with white arrows. Relative intensity is presented below (naïve: $n = 3$, WT or KO DSS treated groups: $n = 4$). (h-i). Gene expression profiling (shown as Heatmap, h) of distal colon tissue from the DSS colitis study comparing WT and uPAR KO mice. Genes displayed are all DSS-induced genes in WT mice (FC > 1.5, $p < 0.05$, total = 192 genes). Detailed expression levels of S100a8, S100a9, Spp1, Mmp13, Il6 and Il1b from the Nanostring analysis of individual animals is shown (i). All data are shown as mean \pm SD and are analysed using 2-way ANOVA followed by Šidák's multiple comparison test (b, d) or 1-way ANOVA followed by Dunnett's multiple comparison test (c, f, g, i).

role of uPAR in DSS-induced inflammation and tissue damage. Taken together, our data show that uPAR deficient mice are more protected from DSS-induced colitis at both histology and gene expression levels, highlighting the therapeutic potential of uPAR in IBD.

Discussion

Epithelial barrier integrity is a critical component of gastrointestinal homeostasis. In IBD, it has been shown that barrier dysfunction precedes the onset of enterocolitis and facilitates disease progression.⁴² Up to now, approaches that protect and/or restore barrier function have gained tremendous research attention. Given that the intestinal epithelial function supplementation in IBD can be regulated by cell surface ligand-receptor interactions, we took a new approach to mine the large public IBD mucosa gene expression datasets and generated new hypotheses based on co-regulated ligand-receptor pairs. We identified a coordinated upregulation of uPAR and its ligand uPA in CD and UC intestinal biopsies, indicating an important role of the ligand-receptor pair in IBD pathogenesis. The high expression of both genes in the anti-TNF-resistant patients also implies that the uPA-uPAR pathway may play an important role in TNF-resistant patients. Overall, our ligand-receptor analysis with high-dimensional IBD datasets provides new opportunities to understand the fundamental biological mechanisms and to identify new targets for IBD treatment.

In addition to the ligand-receptor pair analysis which demonstrates co-ordinated upregulation of uPA and uPAR, we also found that both uPA and uPAR show induced expression during cytokine-induced barrier breakdown in primary human intestinal organoids and reduced expression during barrier formation. Similar regulation of expression was also observed in human Caco-2 intestinal epithelial cells which allow functional studies by genetic approaches. Caco-2 cells deficient of uPAR or uPA that were generated by siRNA KD or CRISPR KO are protected from inflammation-induced barrier dysfunction, as shown by the TEER and permeability assays. Furthermore, uPAR or uPA KO by CRISPR leads to enhanced barrier formation in human Caco-2 epithelial cells. These findings demonstrated a key role of the uPA-uPAR pathway in both damage response and intrinsic barrier function in human cells.

To further validate the function of the uPA-uPAR interaction in human epithelial cells especially in primary human organoid-derived cells, we performed additional pharmacological inhibition studies. Pharmacological inhibition of the uPA-uPAR interaction by the small molecule inhibitor IPR-1110, the neutralizing antibody ab5329, and the peptide antagonists AE234 and AE147, improved barrier function in primary organoid monolayers and in Caco-2 cells. This is independent of the enzymatic function of uPA, since

the uPA protease inhibitor WX-UK1 did not show significant protection during barrier dysfunction. These results argue that uPAR and uPA-uPAR dependent receptor signalling, rather than merely ECM modulation by uPA protease, play a key role in barrier protection. Therefore, small molecule inhibitors or antibodies that target the uPA binding sites on uPAR would be advantageous for IBD therapeutic development. An additional advantage of specifically blocking the uPA-uPAR interaction is that such inhibition avoids potential unwanted side effects of inhibiting the enzymatic function of uPA. Our study focused on cytokine-induced damage in organoids derived from healthy donors. Since uPAR and uPA are significantly upregulated in the intestinal epithelium of IBD patients (Figure S1), future studies using freshly prepared tissue explants from IBD patients will be helpful to further investigate the role of uPAR and uPA in the context of IBD.

Primary intestinal organoids derived from uPAR deficient mice were studied to further confirm our pharmacological inhibition results in primary human organoids. Monolayers derived from uPAR deficient mouse intestinal organoids showed enhanced barrier formation and were protected from cytokine-induced barrier breakdown (Figure 6b-d), which is consistent with the observations in human epithelial cells. Moreover, these mice showed reduced tissue damage and inflammation upon DSS-induced colitis, as measured by histological assessment of mucosal integrity and expression of IBD-associated genes in the mucosal layer. A previous study found that uPAR knock-out mice exhibited exacerbated inflammation in a DSS-colitis model.⁴³ It is noted that our study used a different uPAR KO strain (B6.129P2-*Plaur*^{tm1jd}/J)²⁸ with a different genomic deletion comparing to the strain in the study by *Genua et al.*⁴³ The knock-out mice in our study were genotyped and uPAR expression was validated at the RNA and protein levels (Figure S8a). In addition, we applied 5% DSS in our colitis study, while 2% DSS was used in the study by *Genua et al.*⁴³ It is possible that the pathological role of uPAR in intestinal barrier breakdown is more prominent under severe disease conditions. It should also be noted that in our study, 5% DSS induced expression of well-established IBD markers and the induction of these markers was largely reduced in uPAR deficient mice (Figure 6h). The reduction of intestinal damage upon DSS challenge in the uPAR knockout mice is consistent with the enhanced epi-barrier function in uPAR-deficient intestinal organoids *in vitro* (Figure 6a-d). We also observed an improvement in epithelial tight junction structure in uPAR KO mice after DSS treatment (Figure 6g). These findings also recapitulate our discoveries in human epithelial cells and organoids (Figure 3–4), arguing a conserved function of uPAR in both mouse and human intestinal epithelium. In addition, studies in other epithelial systems also indicated a role for the uPAR pathway in epithelial regulation. For

example, *Swamynathan et al.* showed that SLURP1, a small, secreted protein that affects uPAR function, can stabilize corneal epithelial integrity.⁴⁴ Further investigations with mice in which uPAR is deleted specifically in intestinal epithelial cells will provide additional insight into the role of uPA-uPAR in epithelial regulation. Pharmacological inhibition approaches in various colitis mouse models will further build confidence in therapeutically targeting uPAR for IBD. One limitation of our study is a lack of potent tool inhibitors of mouse uPA-uPAR interaction. A monoclonal antibody, and/or a potent small molecule inhibitor which blocks mouse uPA-uPAR interaction will be necessary to achieve a better understanding of the therapeutic effects *in vivo*.

As a GPI-anchored protein, uPAR functions through additional interactions with cell surface proteins/co-receptors. In this study we confirmed the interaction between uPAR and integrin subunits ($\alpha 5$, $\beta 1$ and $\beta 3$) and EGFR in intestinal epithelial cells through co-IP approaches. Furthermore, we found that uPAR interaction with all three integrin subunits decreases after barrier damage while the EGFR binding remains. EGFR signalling is a key epithelial regulator. It is involved in various cellular activities such as cell survival, cell junctions, mucin secretion and microbiome communications.⁴⁵ In this study, we found that uPAR inhibition leads to improved tight junctions and epithelial cell survival, which could be achieved through, directly or indirectly, modulating EGFR signalling. However, many questions remain unanswered, such as the specific binding site of uPAR-EGFR interaction, how uPA binding to uPAR inhibits EGFR signalling and what are other interaction partners of uPAR. A comprehensive analysis of uPA-uPAR interactome before and after barrier damage would provide insights to further dissect the signalling complex in response to tissue damage.

In summary, we identified the uPA-uPAR ligand-receptor pair as a critical regulator in intestinal barrier integrity. Both uPA and uPAR showed a coordinated induction in IBD mucosa and during cytokine-induced barrier breakdown of human intestinal organoids. Genetic inhibition of uPAR or uPA and pharmacological inhibition of the uPA-uPAR interaction improve barrier function, indicating that uPA-uPAR is a potential IBD target for preventing intestinal barrier breakdown and promoting mucosal healing.

Declaration of interests

During the study, all the authors were Boehringer Ingelheim employees. No author has any further financial, professional, or personal disclosures.

Contributors

Y.C., D.S., J.P.G., L.M. and J.L. designed research; Y.C., T.R.H., X.X., I.Y., and J.Z. performed research; F.S. and

M.H. contributed reagents/analytical tools; Y.C., X.X., I.Y., D.S. and J.Z. analysed data; Y.C. and J.L. wrote the manuscript. Y.C., T.R.H., X.X., D.S., J. Z. and J.L. verified the underlying data. All authors verified the data and approved the final version of the manuscript.

Acknowledgements

We thank Dr. Yi-Hsien Chen and Zhihong Zhang (Genome Engineering & iPSC Centre, Washington University at St. Louis) for assisting the gene editing in Caco-2 cells and Steve Fogal at Boehringer Ingelheim for coordinating mouse breeding and reagents transfer. We are also grateful to Dr. Kathryn Juchem at Boehringer Ingelheim for manuscript editing. The study was supported by Boehringer Ingelheim Pharmaceutical Inc.

Data sharing statement

All data needed to evaluate the conclusions in the paper are present in the paper and/or the Supplementary Materials. Additional data related to this paper may be requested from the corresponding author.

Supplementary materials

Supplementary material associated with this article can be found, in the online version, at [doi:10.1016/j.ebiom.2021.103758](https://doi.org/10.1016/j.ebiom.2021.103758).

Reference

- Konig J, Wells J, Cani PD, Garcia-Rodenas CL, MacDonald T, Mercenier A, et al. Human intestinal barrier function in health and disease. *Clin Transl Gastroenterol* 2016;7(10):e196.
- McGuckin MA, Eri R, Simms LA, Florin TH, Radford-Smith G. Intestinal barrier dysfunction in inflammatory bowel diseases. *Inflamm Bowel Dis* 2009;15(1):100–13.
- Groschwitz KR, Hogan SP. Intestinal barrier function: molecular regulation and disease pathogenesis. *J Allergy Clin Immunol* 2009;124(1):3–20. quiz 1–2.
- Neurath MF, Travis SP. Mucosal healing in inflammatory bowel diseases: a systematic review. *Gut* 2012;61(11):1619–35.
- Neurath MF. New targets for mucosal healing and therapy in inflammatory bowel diseases. *Mucosal Immunol* 2014;7(1):6–19.
- Pineton de Chambrun G, Peyrin-Biroulet L, Lemann M, Colombel JF. Clinical implications of mucosal healing for the management of IBD. *Nat Rev Gastroenterol Hepatol* 2010;7(1):15–29.
- Andrews C, McLean MH, Durum SK. Cytokine tuning of intestinal epithelial function. *Front Immunol* 2018;9:1270.
- Boyapati RK, Rossi AG, Satsangi J, Ho GT. Gut mucosal DAMPs in IBD: from mechanisms to therapeutic implications. *Mucosal Immunol* 2016;9(3):567–82.
- Zundler S, Becker E, Weidinger C, Siegmund B. Anti-adhesion therapies in inflammatory bowel disease-molecular and clinical aspects. *Front Immunol* 2017;8:891.
- Martini E, Krug SM, Siegmund B, Neurath MF, Becker C. Mend your fences: the epithelial barrier and its relationship with mucosal immunity in inflammatory bowel disease. *Cell Mol Gastroenterol Hepatol* 2017;4(1):33–46.
- Marchiando AM, Shen L, Graham WV, Edelblum KL, Duckworth CA, Guan Y, et al. The epithelial barrier is maintained by *in vivo* tight junction expansion during pathologic intestinal epithelial shedding. *Gastroenterology* 2011;140(4):1208–18. e1–2.
- Kawashima R, Kawamura YI, Oshio T, Son A, Yamazaki M, Hagiwara T, et al. Interleukin-13 damages intestinal mucosa via TWEAK

- and Fn14 in mice—a pathway associated with ulcerative colitis. *Gastroenterology* 2011;141(6):2119–29. e8.
- 13 Blasi F, Carmeliet P. uPAR: a versatile signalling orchestrator. *Nat Rev Mol Cell Biol* 2002;3(12):932–43.
 - 14 Crippa MP. Urokinase-type plasminogen activator. *Int J Biochem Cell Biol* 2007;39(4):690–4.
 - 15 Song C, Tseng GC. Hypothesis setting and order statistic for robust genomic meta-analysis. *Ann Appl Stat* 2014;8(2):777–800.
 - 16 Orchard S, Ammari M, Aranda B, Breuza L, Briganti L, Broackes-Carter F, et al. The MIntAct project—IntAct as a common curation platform for 11 molecular interaction databases. *Nucleic Acids Res* 2014;42(Database issue):D358–63.
 - 17 Schaefer MH, Lopes TJ, Mah N, Shoemaker JE, Matsuoka Y, Fontaine JF, et al. Adding protein context to the human protein-protein interaction network to reveal meaningful interactions. *PLoS Comput Biol* 2013;9(1):e1002860.
 - 18 McDowall MD, Scott MS, Barton GJ. PIPs: human protein-protein interaction prediction database. *Nucleic Acids Res* 2009;37(Database issue):D651–6.
 - 19 Chatr-Aryamontri A, Breitkreutz BJ, Oughtred R, Boucher L, Heinicke S, Chen D, et al. The BioGRID interaction database: 2015 update. *Nucleic Acids Res* 2015;43(Database issue):D470–8.
 - 20 Rahmati S, Abovsky M, Pastrello C, Jurisica I. pathDIP: an annotated resource for known and predicted human gene-pathway associations and pathway enrichment analysis. *Nucleic Acids Res* 2017;45(D1):D419–D26.
 - 21 Efremova M, Vento-Tormo M, Teichmann SA, et al. CellPhoneDB: inferring cell–cell communication from combined expression of multi-subunit ligand–receptor complexes. *Nat Protoc* 2020;15(14):1484–1506.
 - 22 Sato T, Stange DE, Ferrante M, Vries RG, Van Es JH, Van den Brink S, et al. Long-term expansion of epithelial organoids from human colon, adenoma, adenocarcinoma, and Barrett's epithelium. *Gastroenterology* 2011;141(5):1762–72.
 - 23 Moorefield EC, Blue RE, Quinney NL, Gentzsch M, Ding S. Generation of renewable mouse intestinal epithelial cell monolayers and organoids for functional analyses. *BMC Cell Biol* 2018;19(1):15.
 - 24 Gardsvoll H, Jacobsen B, Kriegbaum MC, Behrendt N, Engelholm L, Ostergaard S, et al. Conformational regulation of urokinase receptor function: impact of receptor occupancy and epitope-mapped monoclonal antibodies on lamellipodia induction. *J Biol Chem* 2011;286(38):33544–56.
 - 25 Setyono-Han B, Sturzebecher J, Schmalix WA, Muehlenweg B, Sieuwerts AM, Timmermans M, et al. Suppression of rat breast cancer metastasis and reduction of primary tumour growth by the small synthetic urokinase inhibitor WX-UKI. *Thromb Haemost* 2005;93(4):779–86.
 - 26 Liu D, Zhou D, Wang B, Knabe WE, Meroueh SO. A new class of orthosteric uPAR/uPA small-molecule antagonists are allosteric inhibitors of the uPAR/vitronectin interaction. *ACS Chem Biol* 2015;10(6):1521–34.
 - 27 Llinas P, Le Du MH, Gardsvoll H, Dano K, Ploug M, Gilquin B, et al. Crystal structure of the human urokinase plasminogen activator receptor bound to an antagonist peptide. *EMBO J* 2005;24(9):1655–63.
 - 28 Bugge TH, Suh TT, Flick MJ, Daugherty CC, Romer J, Solberg H, et al. The receptor for urokinase-type plasminogen activator is not essential for mouse development or fertility. *J Biol Chem* 1995;270(28):16886–94.
 - 29 Kojouharoff G, Hans W, Obermeier F, Mannel DN, Andus T, Scholmerich J, et al. Neutralization of tumour necrosis factor (TNF) but not of IL-1 reduces inflammation in chronic dextran sulphate sodium-induced colitis in mice. *Clin Exp Immunol* 1997;107(2):353–8.
 - 30 West NR, Hegazy AN, Owens BMJ, Bullers SJ, Linggi B, Buonocore S, et al. Oncostatin M drives intestinal inflammation and predicts response to tumor necrosis factor-neutralizing therapy in patients with inflammatory bowel disease. *Nat Med* 2017;23(5):579–89.
 - 31 Reinisch W, Hung K, Hassan-Zahraee M, Cataldi F. Targeting endothelial ligands: ICAM-1/alicaforfen, MAdCAM-1. *J Crohns Colitis* 2018;12(suppl_2):S669–S77.
 - 32 Arijis I, De Hertogh G, Lemaire K, Quintens R, Van Lommel L, Van Steen K, et al. Mucosal gene expression of antimicrobial peptides in inflammatory bowel disease before and after first infliximab treatment. *PLoS One* 2009;4(11):e7984.
 - 33 Howell KJ, Kraiczky J, Nayak KM, Gasparetto M, Ross A, Lee C, et al. DNA methylation and transcription patterns in intestinal epithelial cells from pediatric patients with inflammatory bowel diseases differentiate disease subtypes and associate with outcome. *Gastroenterology* 2018;154(3):585–98.
 - 34 Schnoor M, Betanzos A, Weber DA, Parkos CA. Guanylate-binding protein-1 is expressed at tight junctions of intestinal epithelial cells in response to interferon-gamma and regulates barrier function through effects on apoptosis. *Mucosal Immunol* 2009;2(1):33–42.
 - 35 Yamaoka T, Yan F, Cao H, Hobbs SS, Dise RS, Tong W, et al. Trans-activation of EGF receptor and ErbB2 protects intestinal epithelial cells from TNF-induced apoptosis. *Proc Natl Acad Sci U S A* 2008;105(33):11772–7.
 - 36 Kim Y, Quach A, Das S, Barrett KE. Potentiation of calcium-activated chloride secretion and barrier dysfunction may underlie EGF receptor tyrosine kinase inhibitor-induced diarrhea. *Physiol Rep* 2020;8(13):e14490.
 - 37 Zhang S, Xu W, Wang H, Cao M, Li M, Zhao J, et al. Inhibition of CREB-mediated ZO-1 and activation of NF-kappaB-induced IL-6 by colonic epithelial MCT4 destroys intestinal barrier function. *Cell Prolif* 2019;52(6):e12673.
 - 38 Sipponen T, Kolho KL. Fecal calprotectin in diagnosis and clinical assessment of inflammatory bowel disease. *Scand J Gastroenterol* 2015;50(1):74–80.
 - 39 Neuman MG. Osteopontin biomarker in inflammatory bowel disease, animal models and target for drug discovery. *Dig Dis Sci* 2012;57(6):1430–1.
 - 40 Vandenbroucke RE, Dejonckheere E, Van Hauwermeiren F, Lodens S, De Rycke R, Van Wouterghem E, et al. Matrix metalloproteinase 13 modulates intestinal epithelial barrier integrity in inflammatory diseases by activating TNF. *EMBO Mol Med* 2013;5(7):1000–16.
 - 41 Friedrich M, Pohin M, Powrie F. Cytokine networks in the pathophysiology of inflammatory bowel disease. *Immunity* 2019;50(4):992–1006.
 - 42 Moore SA, Nighth P, Reyes C, Rawat M, McKee J, Lemon D, et al. Intestinal barrier dysfunction in human necrotizing enterocolitis. *J Pediatr Surg* 2016;51(12):1907–13.
 - 43 Genua M, D'Alessio S, Cibella J, Gandelli A, Sala E, Correale C, et al. The urokinase plasminogen activator receptor (uPAR) controls macrophage phagocytosis in intestinal inflammation. *Gut* 2015;64(4):589–600.
 - 44 Swamynathan S, Swamynathan SK. SLURP-1 modulates corneal homeostasis by serving as a soluble scavenger of urokinase-type plasminogen activator. *Invest Ophthalmol Vis Sci* 2014;55(10):6251–61.
 - 45 Tang X, Liu H, Yang S, Li Z, Zhong J, Fang R. Epidermal growth factor and intestinal barrier function. *Mediators Inflamm* 2016;2016:1927348.